Nucleolar Assembly of the rRNA Processing Machinery in Living Cells

Tulia Maria Savino,* Jeannine Gébrane-Younès,* Jan De Mey,‡ Jean-Baptiste Sibarita,§ and Danièle Hernandez-Verdun*

*Institut Jacques Monod, UMR 7592, 75251 Paris, France; ‡Institut Curie/Section de Recherche, UMR 146, 91405 Orsay, France; and §Institut Curie/Section de Recherche, UMR 144, 75248 Paris, France

Abstract. To understand how nuclear machineries are targeted to accurate locations during nuclear assembly, we investigated the pathway of the ribosomal RNA (rRNA) processing machinery towards ribosomal genes (nucleolar organizer regions [NORs]) at exit of mitosis. To follow in living cells two permanently transfected green fluorescence protein–tagged nucleolar proteins, fibrillarin and Nop52, from metaphase to G1, 4-D time-lapse microscopy was used. In early telophase, fibrillarin is concentrated simultaneously in prenucleolar bodies (PNBs) and NORs, whereas PNB-containing Nop52 forms later. These distinct PNBs assemble at the chromosome surface. Analysis of PNB movement does not reveal the migration of PNBs towards the nucleolus, but rather a directional flow between PNBs and between PNBs and the nucleolus, ensuring progressive delivery of proteins into nucleoli. This delivery appeared organized in morphologically distinct structures visible by electron microscopy, suggesting transfer of large complexes. We propose that the temporal order of PNB assembly and disassembly controls nucleolar delivery of these proteins, and that accumulation of processing complexes in the nucleolus is driven by pre-rRNA concentration. Initial nucleolar formation around competent NORs appears to be followed by regroupment of the NORs into a single nucleolus 1 h later to complete the nucleolar assembly. This demonstrates the formation of one functional domain by cooperative interactions between different chromosome territories.

Key words: nuclear dynamics • electron microscopy • prenucleolar body • time-lapse microscopy • 4-D imaging

Introduction

The reinitiation of transcriptional and processing activities at the end of mitosis requires preassembled complexes passing through mitosis. Some of these complexes travel in association with chromosomes before being redistributed at their sites of activity. As specific delivery of these complexes is fundamental, their sorting as well as their traffic in the nucleus is an important process in the establishment of nuclear function. However, at present there is very little information in living cells concerning the pathway followed by components of the transcriptional and processing complexes at the onset of nuclear formation.

The nucleolus is the prototype of an active nuclear domain that assembles at the end of mitosis and is crucial for the organization of important nuclear functions. It is the site where the ribosomal genes (rDNAs) are transcribed, and the ribosomal RNAs (rRNAs)[1] processed and associated with ribosomal proteins (for reviews, see Hadjiolov, 1985; Shaw and Jordan, 1995; Scheer and Hock, 1999). It is also a plurifunctional nuclear domain (Pederson, 1998; Olson et al., 2000) involved in cell cycle control (Visitin and Amon, 2000), nuclear protein export (Zolotukhin and Felber, 1999), and the aging process (Guarente, 1997), and it also contains components of signal recognition particles (Politz et al., 2000).

From past investigations the general concept emerges that nucleolar assembly is mainly a two-step process (Scheer et al., 1993; Thiry and Goessens, 1996). The first step involves activation of the transcription machinery which depends on the decrease of Cdk1-cyclin B activity (Sirri et al., 2000). Moreover, the RNA polymerase I (RNA pol I) transcription machinery is not delocalized during mitosis but remains associated with the genes in nucleolar organizer regions (NORs; Jordan et al., 1996; Roussel et al., 1996; Gébrane-Younès et al., 1997; Sirri et al., 1999). The second step corresponds to recruitment of the processing

The online version of this article contains supplemental material.

Address correspondence to D. Hernandez-Verdun, Institut Jacques Monod, 2 Place Jussieu, 75251 Paris Cedex 05, France. Tel.: 331-44-27-40-38. Fax: 331-44-27-59-94. E-mail: dhernand@ccr.jussieu.fr

[1]*Abbreviations used in this paper:* DFC, dense fibrillar component; GC, granular component; GFP, green fluorescence protein; ITS, internal transcribed spacer; NDF, nucleolus-derived foci; NOR, nucleolar organizer region; PNB, prenucleolar body; PSF, point spread function; RNA pol I, RNA polymerase I; rRNA, ribosomal RNA; 3-D, three-dimensional; UBF, upstream binding factor.

machinery in the nucleolus via the formation of prenucleolar bodies (PNBs). These PNBs were described as mobile nuclear bodies participating in the delivery of the processing machinery at the sites of rDNA transcription. This notion is based on immunolocalization in fixed cells (Ochs et al., 1985; Benavente, 1991; Jiménez-Garcia et al., 1994; Fomproix et al., 1998; Savino et al., 1999). It has been proposed that the translocation of PNBs at NORs depends on the activation of transcription, but not PNB formation itself (Benavente, 1991). However, it was also found that the regroupment of PNBs associated with pre-rRNAs into the nucleolar sites can take place in the absence of active RNA pol I transcription (Verheggen et al., 1998; 2000). Similarly, inhibition of RNA pol I transcription by actinomycin D does not prevent the recruitment of nucleolar proteins at NORs whereas PNBs seem to be stabilized in the nucleoplasm (Dousset et al., 2000).

Many questions concerning the formation of the nucleolus and, in particular, how PNBs are involved in the nuclear traffic occurring in living cells at the time of nucleolar assembly, could be answered if the dynamics of the process were analyzed in living cells at the transition between mitosis and interphase. In a recent study, it was reported that as the cells progressed through telophase, the fibrillarin-green fluorescence protein (GFP) signal from the PNBs decreased with a concomitant increase in the intensity of nucleolar fluorescence (Dundr et al., 2000). PNBs were seen not to be mobile, and the establishment of direct contacts between PNB extensions and nucleolus were also noted. However, on the basis of fluorescence recovery after photobleaching, the authors suggested a diffusion mechanism to explain the transfer of PNB components to newly forming nucleoli (Dundr et al., 2000). Similarly during interphase, and using the same approach, it has been proposed that nuclear and nucleolar proteins diffuse within the nuclear volume (Phair and Misteli, 2000). However, data supporting the hypothesis of a specific pathway for newly assembled small nuclear ribonucleoproteins (snRNPs) were also reported (Sleeman and Lamond, 1999; Platani et al., 2000). These two mechanisms, diffusion or a specific nuclear pathway, are not necessarily exclusive but presumably should also integrate different kinds of nuclear bodies involved in the traffic of preassembled complexes (Isaac et al., 1998; Matera, 1999; Sleeman and Lamond, 1999; Eils et al., 2000; Platani et al., 2000). In any case, in order to be able to conclude on the mechanisms of nuclear traffic in living cells, it is important to analyze the nuclear traffic in the nuclear volume and not in one optical section.

PNBs are preassembled complexes composed of nucleolar proteins and small nucleolar RNAs involved in rRNA processing. It has been proposed that there are several types of PNBs dedicated to early or late events (Fomproix and Hernandez-Verdun, 1999; Mukharyamova et al., 1999; Savino et al., 1999; Verheggen et al., 2000). To understand the in vivo traffic of different preassembled complexes at the time of nuclear assembly after mitosis, we tagged with GFP two nucleolar proteins which associate with PNBs, fibrillarin, and Nop52. Both proteins are found at the chromosome periphery during mitosis and are subsequently targeted to the nucleoli (Fomproix et al., 1998; Savino et al., 1999). Fibrillarin participates in early processing of rRNA, i.e. processing of the 5′ external transcribed spacer (5′ETS) and localizes in the dense fibrillar component (DFC) of the nucleolus, whereas Nop52 is associated with late events related to the removal of the second internal transcribed spacer (ITS2) and localizes in the granular component (GC) of the nucleolus. Here, using three-dimensional (3-D) time-lapse microscopy (4-D imaging) and electron microscopy analysis, we demonstrate that distinct PNBs which form on the chromosome surface are involved in fibrillarin and Nop52 traffic. We further show that during telophase and early G1, these PNBs serve as transient assemblies and transit sites for nucleolar components without being mobile themselves.

Materials and Methods

Plasmids

The cDNA corresponding to Nop52 was excised from a plasmid described previously (Savino et al., 1999). The EcoRI sites at both termini were used for in frame subcloning of Nop52 into the pEGFP-C2 EcoRI sites (CLONTECH Laboratories, Inc.); pEGFP-C2 contains an enhanced GFP mutant under the control of the cytomegalovirus (CMV) promoter and a G-418 resistance gene. The full-length fibrillarin cDNA, a gift from J.P. Aris (Department of Anatomy and Cell Biology, University of Florida, Gainesville, FL) (Aris and Blobel, 1991) was excised from pBluescript; it was inserted in frame in the PstI and ApaI sites of pEGFP-C2.

Cell Culture and Obtention of Stable Transfected Cell Lines

HeLa cells were cultured in Eagle's minimum essential medium (Sigma-Aldrich) supplemented with 10% FCS and 2 mM L-glutamine (GIBCO BRL).

HeLa cells were transfected at 60% confluence using the Superfect reagent (QIAGEN) following the manufacturer's instructions. Selection of stable transfected cells was carried out by treatment with G-418 sulfate (800 μg/ml; Life Technologies). After 15 d under the selection pressure, drug-resistant cells were sorted by flow cytometry according to expression levels. For Nop52-GFP, only one cell was plated per well. A clone that presented a normal cell cycle and high expression levels was used. For fibrillarin-GFP, a stable cell line was also obtained by successive sorting by flow cytometry.

Antibodies

Antibodies with the following specificities were used: a mouse monoclonal anti-fibrillarin, 72B9 (Reimer et al., 1987), a human serum C13 containing specific autoantibodies against Nop52 (Savino et al., 1999), a human serum against upstream binding factor (UBF; A17) (Roussel et al., 1993), and mouse monoclonal antibodies against GFP (Roche). A human serum against fibrillarin, GM4, was used for Western blotting (Fomproix et al., 1998). Anti–mouse secondary antibodies, conjugated to FITC or to Cy3, anti–human antibodies conjugated to Cy5, and goat antibodies conjugated to Texas Red were purchased from Jackson ImmunoResearch Laboratories. For Western blotting, peroxidase-conjugated goat anti–human and anti–mouse antibodies (Jackson ImmunoResearch Laboratories) were used.

Immunofluorescence

For immunofluorescence, cells were grown as monolayers on glass coverslips, fixed in 2% (wt/vol) paraformaldehyde for 20 min at room temperature, and permeabilized with 0.5% Triton X-100 for 5 min. Cells were incubated at room temperature for 60 min in PBS with the first antibody and then for 60 min with the secondary antibody. Samples were stained with the DNA-specific 4′,6-diamino-2-phenylindole (DAPI; Sigma-Aldrich) dye. All preparations were mounted with the antifading solution Citifluor (CITIFLUOR, Ltd.).

Assay of RNA Pol I Activity In Situ (Run On)

The run on assay was performed on HeLa cells grown as monolayers, essentially as described (Roussel et al., 1996) in conditions set up to reveal RNA

pol I transcription (Moore and Ringertz, 1973). BrUTP incorporation was detected by immunofluorescence labeling using a mouse anti-bromodeoxyuridine monoclonal antibody (Roche) revealed by FITC-conjugated goat anti–mouse antibodies (Jackson ImmunoResearch Laboratories).

Immunoblotting

For protein analysis, control HeLa cells, fibrillarin-GFP, and Nop52-GFP transfected HeLa cell lines were solubilized in SDS sample buffer and analyzed by 10% SDS-PAGE. Immunoblotting was as described (Savino et al., 1999). Detection of immunoreactive bands was performed by chemiluminescence using peroxidase-conjugated antibodies and the supersignal kit (Pierce Chemical Co.) as enhancer, following the manufacturer's instructions. Membranes were exposed to a Fuji X-ray film (Fuji Photo Film Co. Ltd.). The membranes were dehybridized by incubation in 62.5 mM Tris-HCl, 100 mM β-mercaptoethanol, and 2% SDS for 30 min at 60°C, and then washed with PBS for subsequent immunoblotting.

Microscopy 3-D and 4-D Acquisition System

Pictures of fixed cells were collected using a 3-D deconvolution imaging system, whose detailed description and validation will be published elsewhere (Sibarita and De Mey, in preparation). In brief, it consisted of a Leica DM RXA microscope, equipped with a piezoelectric translator (PIFOC; PI) placed at the base of a 100× PlanApo N.A. 1.4 objective, and a 5 MHz Micromax 1300Y interline CCD camera (Roper Instruments). For the acquisition of Z-series, the streaming mode allows the camera to operate at full speed by controlling the piezo translator during the chip readout. Stacks of conventional fluorescence images were collected automatically at 0.2 μm Z-distance (Metamorph software; Universal Imaging Corp.). Wavelength selection was achieved by switching to the corresponding motorized selective Leica filter block before each stack acquisition. Exposure times were adjusted to provide circa 3000 grey levels at sites of strong labeling. Automated batch deconvolution of each Z-series was computed using a measured point spread function (PSF) with a custom-made software package (J.B. Sibarita, Institut Curie/Section de Recherche). The PSF of the optical system was extracted from 3-D images of fluorescent beads of 0.1 μm of diameter (Molecular Probes) collected at each wavelength. The high signal to noise ratio (SNR) of the data sets lead us to use iterative constrained deconvolution algorithms (Meinel, 1986), commonly used in the field of microscopy (Agard et al., 1989). They are issued from the classical imaging equation: $i = o \otimes h + n$, where i, o, h and n represent, respectively, the acquisition, the object one wishes to compute, the PSF, and the noise. In this class of algorithm the noise is neglected. The classical imaging equation can then be simplified and extended to its iterative form, from which various algorithms can be derived. We have chosen to use the multiplicative correction algorithm, described in its discrete formulation below, because of its rapid convergence, well suited for large data sets:

$$o_m^{(k+1)} = K o_m^{(k)} \frac{i_m}{\sum_l h_{m-l} o_l^{(k)}},$$

with $o^o = i$, and where $o^{(k+1)}$ and $o^{(k)}$ are, respectively, the new and the previous estimates. To control the noise and avoid artefacts during the iterative process, we apply a gaussian filtering to the first estimate and every 5 to 7 iterations, depending on the noise level. Typically, deconvolution of a stack 400 × 400 × 50 takes 90 s per color on a Pentium III-866 MHz.

Live cell 4-D microscopy was carried out using a novel imaging system, also capable of performing fast 5-D imaging (3-D plus 2 fluorophores plus time), whose detailed description and validation will be published elsewhere (De Mey and Sibarita, in preparation). In brief, it uses a bottom port Leica DM IRBE microscope. A piezoelectric translator controlled by a 5 MHz Micromax 872Y interline CCD camera (Princeton Instruments) assures rapid and reproducible Z-stepping in stream mode. Shuttering and illumination was assured by a 175 W Xenon lamp housed in a Sutter DG4 illuminator linked to the microscope by an optical fiber. For GFP imaging, a Leica GFP filter block was used. Stacks of images with a Z-step of 0.3 μm were acquired with a 100× PlanApo N.A. 1.4 oil immersion objective in stream mode (Metamorph) using the camera set at 2 × 2 binning. Each stack of 10 to 50 images was acquired in 1 to a few seconds with a frequency ranging from every 5 s to every 2.5 min. The number of images per stack was based on the exposure time in order to obtain entire stacks in <2 s. The cells were grown on glass coverslips, 18 mm in diameter, and mounted in a Ludin observation chamber (LIS). During live observation the chamber was filled with 10 mM Hepes, pH 7.4, in complete medium. The entire microscope and the chamber were kept at 37°C by a microscope incubator (LIS). All stacks were treated by automatic batch deconvolution (J.B. Sibarita). The PSF of the optical system was extracted from 3-D images of green fluorescent beads of 0.1 μm of diameter (Molecular Probes). For rapid 4-D imaging, Z-sections need to be acquired as fast as possible to be compatible with deconvolution; structures need to remain immobile over several Z-sections in order to reassign the light to its original place. Moreover, illumination and exposure time need to be decreased at maximum, in order to keep the cells alive and avoid photobleaching. Consequently, in most of the cases, recorded images have a poor signal to noise ratio and noise cannot be neglected in the deconvolution process. As the noise present in the images follows a Poisson law, we decided to use the Richardson-Lucy deconvolution algorithm, based on the maximization of the likelihood for a Poisson process (Richardson, 1972). Its discrete formulation is the following:

$$o_m^{(k+1)} = K o_m^{(k)} \sum_l h_{m-l} \frac{i_l}{\sum_n h_{l-n} o_n^{(k)}}.$$

This iterative algorithm gives the new estimate $o^{(k+1)}$ of the object we want to observe as a function of the previous estimate $o^{(k)}$, the recorded image i, and the PSF h. Typically, deconvolution of a stack 400 × 400 × 50 takes 180 s on a Pentium III-866 MHz.

3-D and 4-D pseudocolored overlays and 3-D stereoscopic projections and animations were generated using Metamorph. Surface rendering and volume quantifications were performed using Amira software (TGS).

Transmission Electron Microscopy

HeLa cells were grown on microgrid coverslips (CELLocate; Eppendorf), the alphanumeric labeling of the grids facilitating the location of individual cells by light microscopy. The cells were treated in situ according to published procedures (Gébrane-Younès et al., 1997). In brief, cells were fixed in 2% (wt/vol) paraformaldehyde, 2.5% (vol/vol) glutaraldehyde in 0.1 M sodium cacodylate buffer, pH 7.4, at 4°C for 30 min, rinsed, postfixed in 1% (wt/vol) osmium tetroxide in the same buffer, dehydrated, and embedded in Epon 812. After resin polymerization, the embedded cells were separated from the microgrid coverslips carrying the imprint of the alphanumeric labeling. By light microscopy cell cycle phases from telophase and G1 were identified and located using the grid marks. Ultrathin sections of these cells were conventionally contrasted with uranyl acetate (10 min) followed by lead citrate (5 min) and examined in a Philips CM12 electron microscope.

Combined Fluorescence and Electron Microscopy

Some PNBs were successively observed by fluorescence and electron microscopy in the same cells. For this purpose, stably transfected Nop52-GFP HeLa cells grown on microgrid coverslips were fixed in 4% paraformaldehyde in PBS. After recording the fluorescence signals and the position of the selected cells on the microgrid coverslips, the cells were treated as described above (glutaraldehyde and osmium tetroxide fixations before Epon embedding). Ultrathin serial sections (110 nm) of the cells were mounted onto single slot formvar-coated copper grids, contrasted, and observed as above.

Online Supplemental Material

Videos corresponding to Figs. 2–6 and Fig. 9 are presented. Image sequences were animated as Quicktime files using Adobe Premiere. Online supplemental material available at http://www.jcb/org/cgi/content/full/153/4/1097/DC1.

Video 1: recruitment of Nop52 in PNBs and nucleoli. Projection of 15 focal planes, acquisition frequency: every 15 s. In a high magnification the protein flow between PNB and the nucleolus is indicated by arrows.

Video 2: assembly of fibrillarin in PNBs and NORs. A 3-D rotation of the cell is shown at different stages. Projection of 33 focal planes, acquisition frequency: every 30 s.

Video 3: video 1 and video 2 were run in parallel. Both videos are shown with a frequency of every 30 s. Note that the acquisition for fibrillarin starts 2 min later.

Video 4: (A) recruitment of Nop52 during telophase showed by pseudocolored intensity profile. Projection of 25 focal planes, acquisition frequency: every 5 s. High magnification of a developing NOR. (B) Black and white projection of the same cell. At high magnification interconnections between PNBs are observed.

Video 5: a fixed cell is shown by animating the acquisition stack that goes from top to bottom. Nop52 is represented in green, fibrillarin in red, and DNA in blue.

Video 6: the flow of fibrillarin between a PNB and a NOR is shown by coloring the surface of each element.

Video 7: this sequence shows the recruitment of Nop52 in PNBs and NORs, and later the fusion of two nucleoli; a zoom of this fusion is shown. Projection of 25 focal planes, acquisition frequency: every 2′ 30″.

Results

In Transfected Cells, the GFP-tagged Nucleolar Proteins Localize, As Do Endogenous Proteins

Fibrillarin and Nop52 were tagged with GFP and transfected into HeLa cells. Stably transfected fibrillarin-GFP and Nop52-GFP cell lines were established to guarantee a normal physiological situation and consequently the observation of normal pathways. Of these, two clones whose cell cycle timing did not differ from control HeLa cells were used for further experiments.

The GFP-tagged proteins detected by Western blots migrated as single fusion proteins and more slowly than the endogenous proteins due to fusion with the GFP protein (Fig. 1). The total amount of proteins (endogenous and fusion proteins) was higher in transfected cells than in control cells (Fig. 1, compare lanes 1 and 2 and 4 and 5). However, the amount of other nucleolar proteins, i.e., nucleolin and protein B23, was similar in transfected and control HeLa cells (data not shown). This supports the conclusion that the transfected cell lines are not altered.

We next verified that transgene products were targeted similarly to endogenous proteins during mitosis and interphase. No detectable difference was observed in cellular distribution between GFP and antibody signals in control cells (data not shown). The Nop52-GFP signal was seen at the periphery of the chromosomes during mitosis, in nucleoli during interphase, and in PNBs (see below), as shown by Nop52 antibodies in control cells (Savino et al., 1999). Similarly, fibrillarin-GFP was localized at the chromosome periphery, in PNBs, in coiled bodies, and in the nucleolus, as in control cells (data not shown). Consequently, these permanent transfected cell lines can be used to study the dynamics of translocation of nucleolar proteins from the chromosome periphery to the nucleolus during formation of the interphase nucleus.

From Mitosis to G1, the Dynamics of the Nucleolar Proteins Exhibit a Two-Step Redistribution

Our objective was to follow in living cells the translocation of fibrillarin and Nop52 from metaphase to the time where nucleoli were completely assembled in G1. In early G1 cells, nucleolar proteins move within the entire nuclear volume. Furthermore, at the end of mitosis, the chromosomes to which the proteins are still associated are stacked perpendicularly to the substrate, and this volume flattens during early G1. Therefore, the events cannot be followed in only one optical plane. Rather, 3-D time-lapse microscopy enabling rapid acquisitions of Z-stacks at short intervals is required. Using a novel 4-D imaging system (3-D plus time = 4-D imaging), we collected 3-D data sets as described in Materials and Methods.

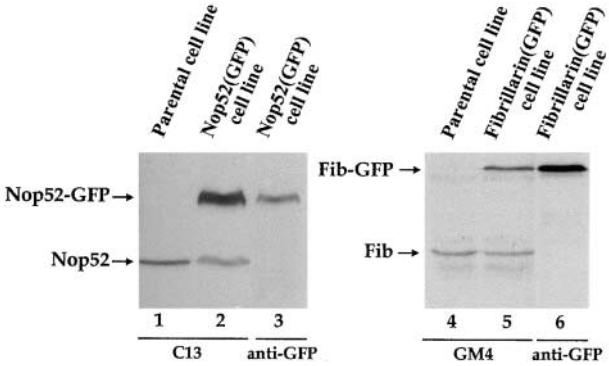

Figure 1. SDS-Page analysis of whole cell lysates of stably transfected and nontransfected HeLa cells. The same number of nontransfected parental cells and Nop52-GFP transfected cells were probed with C13. In lane 1, endogenous Nop52 is detected as a single band of 52 kD. Two bands of 52 and 80 kD were detected in lane 2, Nop52 and Nop52-GFP, respectively. When the blot of lane 2 was probed with anti-GFP, only Nop52-GFP was detected, lane 3. The same number of nontransfected parental cells and fibrillarin (Fib)-GFP transfected cells were probed with GM4 (antifibrillarin antibody). In lane 4, only a 34-kD band corresponding to fibrillarin was detected; in stable fibrillarin-GFP cells, lane 5, two bands of 34 and 65 kD were seen, fibrillarin and fibrillarin-GFP, respectively. When the blot of lane 5 was probed with anti-GFP, only the band corresponding to fibrillarin-GFP was revealed, lane 6.

40 GFP-transfected HeLa cells were recorded from metaphase to nucleolar assembly in interphase. As Nop52 and fibrillarin associated to the chromosome periphery, the mitotic stages were easily determined. Chromosome migration towards the poles took about 4 min after the onset of anaphase. During anaphase migration, the fibrillarin-GFP and the Nop52-GFP signals outlined the chromosomes, showing that Nop52 and fibrillarin traveled in association with chromosomes. After their migration to the poles, the two proteins redistributed into PNBs and NORs, but the behavior of the two proteins was different, in particular with respect to their kinetics to join the NORs (Figs. 2 and 3, and Videos 1 and 2). These observations prompted us to analyze in detail PNB formation and motility in relation to NOR and nucleolar assembly for each protein.

Different Kinetics of PNB Formation at Telophase

As soon as the chromosomes had reached the poles, the cells entered into telophase. Both proteins still formed a faint and continuous sheath around the chromosomes. Strikingly, at that time, bright spots of concentrated fibrillarin-GFP appeared (Fig. 3, from 2′30″, and Video 2). Some of these foci could be identified as NORs, as later they become the sites of nucleolar assembly, whereas other foci corresponded to PNBs (see below). In contrast, it was not before 12 min after the onset of anaphase that the Nop52-GFP signals started to appear as bright foci, which at that moment are exclusively PNBs (Fig. 2, from 12′ 15″, and Video 1 and Video 3 for comparative kinetics). Nop52-GFP containing NORs became visible later, in early G1. Thus, at the end of mitosis, the redistribution of the nucleolar proteins studied here occurs with different kinetics (see also below in fixed cells).

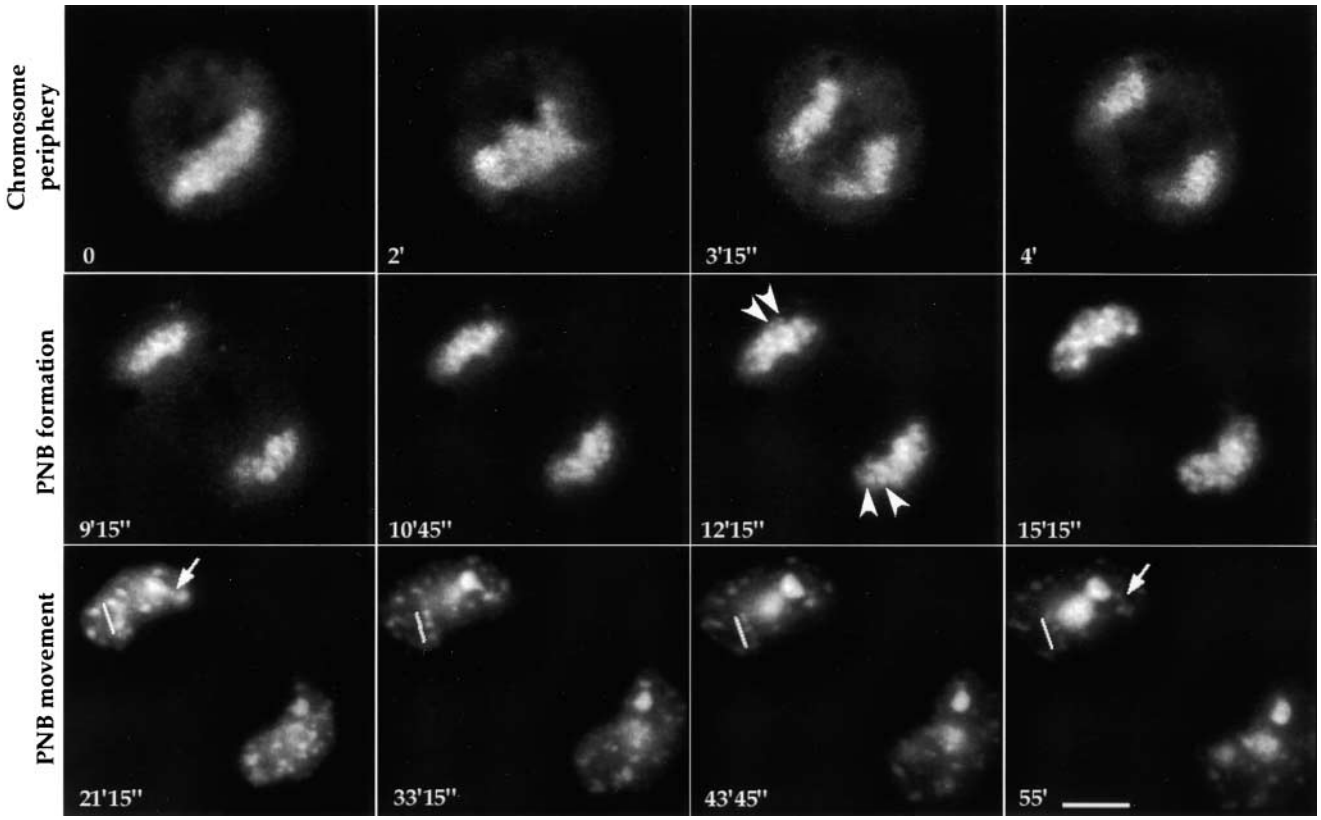

Figure 2. Time-lapse sequence of Nop52-GFP, from mitosis to early G1 phase. Projection of 15 focal planes. Nop52-GFP is found at the periphery of the chromosomes during metaphase (time 0). It follows chromosome movement reaching the poles after 4 min. Between 10 to 15 min, Nop52-GFP is redistributed and concentrates in PNBs (arrowheads). PNBs either display an oscillatory movement in the nucleoplasm, deliver material to incipient nucleoli, or disintegrate on the spot. See also Video 1. 1 h after the beginning of anaphase, Nop52-containing PNBs are still observed. PNB alignments in the nucleoplasm (white lines) and protein flow in the vicinity of nucleoli (arrows) are observed. Bar, 10 μm. See video for nucleolar reconstruction.

Viewing of the films indicates that the PNBs are dynamic structures. We therefore analyzed in detail the kinetics of the Nop52-containing PNBs. Using Metamorph software which represents the fluorescent signal as "altitude curves", we were able to follow the evolution of the signals in individual PNBs. Each PNB displayed a phase of concentration peaking at a certain level before declining (Fig. 4 A and Video 4 A). The PNBs displayed an oscillatory movement about most probably the chromosomes (Fig. 4 A and Video 4 A). This is supported by stereoscopic viewing and image rotations at chosen times which revealed a dynamic distribution in a trabecular network and the progressive formation and disappearance of discrete aligned spots (Fig. 4 B, and enlargements of squares a and b, Video 4 B).

To further characterize the formation of PNBs in telophase, we studied the distribution of fibrillarin and Nop52 in relation with chromosomes by immunofluorescence labeling. As markers of NOR location, the activation of RNA pol I transcription by BrUTP incorporation and the labeling of the transcription factor UBF were used. In 3-D acquisitions of fixed HeLa cells at early telophase, DNA staining clearly outlined the shape and surface of individual chromosomes (Fig. 5 A, three representative optical planes are shown, and Video 5). Typically, Nop52-GFP outlined individual chromosomes (Fig. 5 A″) whereas fibrillarin was mostly associated with NORs (Fig. 5 A′ and merge in 5 A‴) with some foci remaining at the chromosome periphery. The concentration of fibrillarin at the chromosome periphery was much lower than that of Nop52. We proved accumulation of fibrillarin at NORs by colocalization with UBF (Fig. 5 B). In this telophase, accumulation of fibrillarin at NORs is clearly visible, whereas the major location of Nop52 outlines the chromosome periphery. This same pattern of Nop52 distribution is observed when RNA pol I transcription, revealed by BrUTP incorporation, is activated in NORs (Fig. 5 C, see merge). Thus, at the time of reinitiation of transcription, fibrillarin was recruited in the NORs whereas Nop52 was still at the chromosome periphery confirming the different dynamics of these proteins observed by time-lapse microscopy.

As already described (Dundr et al., 1997; 2000), nucleolus-derived foci (NDF) were observed in the cytoplasm at telophase (Figs. 2–5 and 9, and related videos), indicating the presence of NDFs containing fibrillarin-GFP and Nop52-GFP in both transfected cell lines. The motion of these NDFs was very rapid and over long distances. These NDFs contacted the nuclear border after which it became impossible to discriminate them on the basis of their motion, and they could no longer be distinguished from other nucleolar bodies. Recently, it was reported that PNBs in nuclei and NDFs in the cytoplasm have a similar morphology and

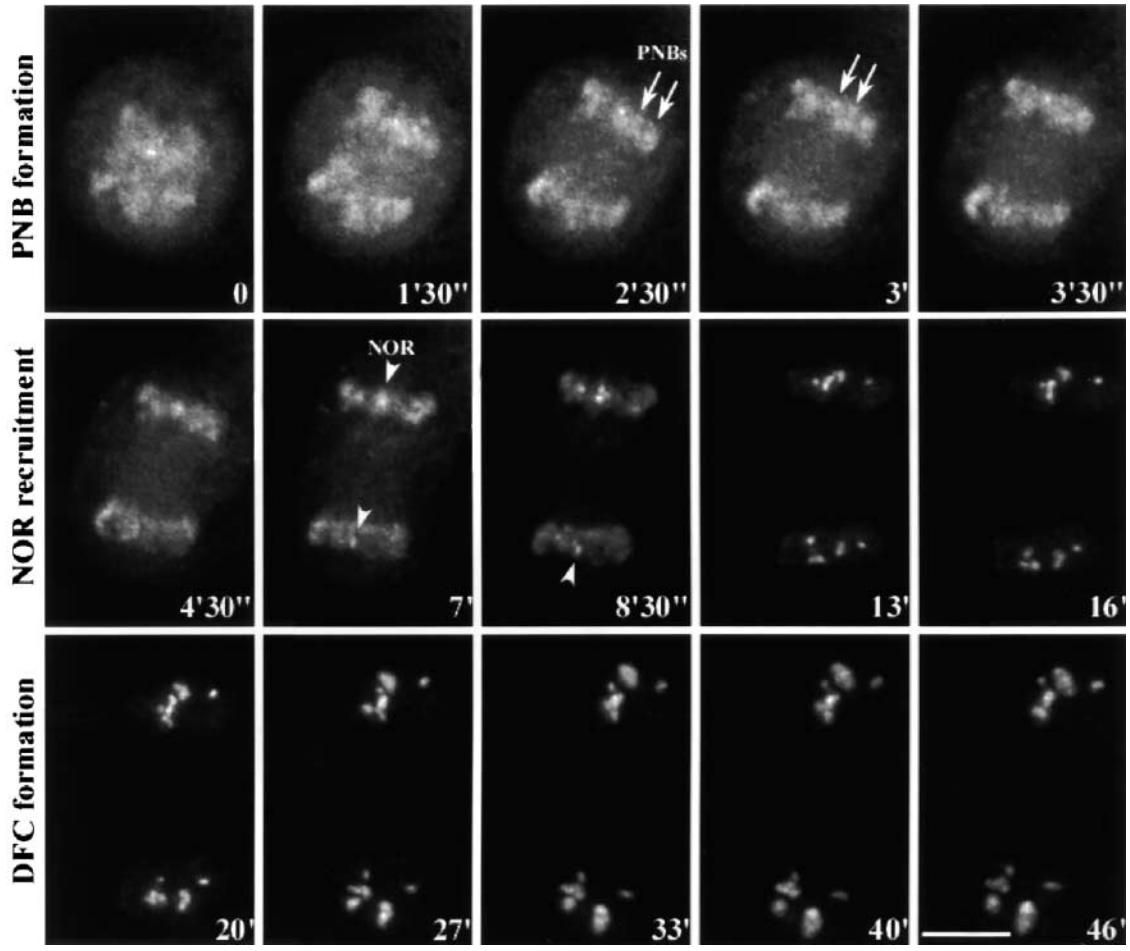

Figure 3. Time-lapse sequence of fibrillarin-GFP, from mitosis to early G1 phase. Projection of 33 focal planes. At 2′30″, fibrillarin starts to assemble in PNBs (arrows). NORs become very distinct at 7 min (arrowheads). In <15 min incipient nucleoli can be seen. Then, the DFC-containing fibrillarin expands progressively (from 20 min). See also Video 2. Note that in this figure, the illustration starts after the onset of anaphase. Time 0 corresponds approximately to 2′30″ after metaphase as evidenced in Video 3. Bar, 10 μm. See also Video 7 (online supplement) for nucleolar reconstruction.

similar recovery after photobleaching (Dundr et al., 2000); they could both participate in the same pathways but direct proof of this possibility is still lacking.

PNB Motion and Protein Delivery into Nucleoli

Time-lapse microscopy showed that about 15–20 min after the beginning of anaphase (Fig. 2), the Nop52-containing PNBs became easily discriminated near the nuclear periphery, and were located in the vicinity of nucleoli or as alignments in the nucleoplasm. The analysis of the motility of these PNBs by following individual PNBs by 4-D imaging and rotation of the 3-D images revealed that they displayed only an oscillatory movement without visible motility towards the nucleolus. Some of the peripheral PNBs were still visible in G1 when nucleoli were assembled, and subsequently simply disappeared without providing evidence supporting the hypothesis of their direct translocation into nucleoli. Analyzing the life time of several individual PNBs, we found that Nop52-containing PNBs are very stable (80 min ± 20 min), whereas fibrillarin-containing PNBs lasted for only 15 min (± 5 min). This reveals for the first time a differential regulation of the persistence of these two types of PNBs.

When analyzing the behavior of PNBs at the time of their dissociation, we detected the existence of "bridges" containing GFP-tagged proteins which link adjacent PNBs (Fig. 6 A). In a time-lapse series, one PNB diminished in intensity, whereas its neighbor or a NOR linked to it by such a bridge increased in intensity (Fig. 6, A–C). Thus, such dynamics suggest the existence of a jet-like flow of tagged proteins from one PNB to another (Fig. 6, and Videos 1, 2, and 6). The flow lasted no more than 2 min and was directional. This flow representing delivery of protein could indicate that the redistribution of the nucleolar material is performed by relay, from one PNB to another. These jet-like flows were also observed in early G1 fixed cells (Fig. 7), indicating a common mechanism during nucleolar reformation.

The oscillatory movement observed for PNBs and their formation at the chromosome periphery in telophase (Figs. 2, 3, and 4, and Videos 1, 2, and 4) prompted us to investigate if the association of PNBs with condensed chromatin is maintained in interphase nuclei. 3-D imaging of fixed early G1 nuclei showed that PNBs were still close to masses of condensed chromatin (Fig. 7). At the resolution of electron microscopy, the first easily identified PNBs at

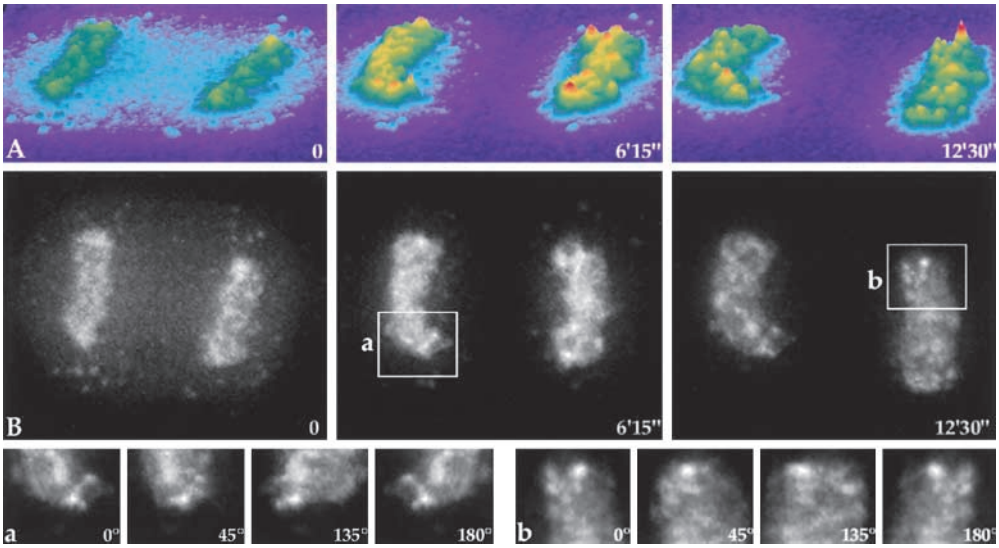

Figure 4. Localization of Nop52 during telophase in time-lapse sequences. Projection of 25 focal planes. Three key steps can be observed, the periphery of the chromosomes (time 0), PNB formation (6′15″), and the recruitment of Nop52 in the NORs (12′30″). These steps are represented by an intensity profile (A) in color and height, low intensity signal in pale blue, and high intensity represented in red by peaks. (B) The same image as in panel A is shown as a two-dimensional projection. Nop52 is found at the periphery of the chromosomes, and in a 3-D image (enlargement of squares a and b) a network is observed, distributed in the interchromatin space, structures become discrete, and protein distributes in foci or PNBs. A projection of different angles is presented in a and b. See also Video 4, A and B, for 4-D PNB formation.

late telophase were found adjacent to condensed chromatin in accordance with the impression obtained when examining fixed and living cells. Some of these PNBs were connected to the condensed chromatin by thin threads (Fig. 8, B and C). These observations in living cells as well as in 3-D fixed cells and at the resolution of electron microscopy are consistent with the fact that PNBs maintained a link with condensed chromatin most probably at the periphery of the chromosome territory. The earliest identified PNBs were 0.1 μm and were composed of dense fibrillar material (Fig. 8 B), whereas late PNBs appeared very dense, containing granules of about 15 nm (Fig. 8 A″, 8 D′, and 8 E). We proved that these late PNBs effectively contain Nop52-GFP by recording the GFP fluorescent signal in early G1 cells (Fig 8, A and A′) followed by observation of the same PNBs by electron microscopy (Fig 8 A″).

In living cells, protein delivery from PNBs to the nucleolus appeared as an oriented flow as shown in Fig. 6, B and C. When Nop52-containing PNBs followed by 4-D imaging approached the nucleoli, they became attached to them without fusing immediately. This created an intermediate structure which persisted for several minutes. Then the PNB material was delivered into nucleoli concomitantly with an increase of the GFP signal in the nucleoli. The results of electron microscopy studies indicate that the bridge is constituted by dense fibrils connecting PNBs and the DFC of nucleoli in late telophase (Fig. 8 B), whereas the late PNBs established contact with the GC of nucleoli (Fig 8, D and E). At the boundary between these PNBs and the nucleolus, PNBs were seen bridged to the GC of the nucleolus by particles of lower electron density (Fig. 8, D′ and E). Moreover the presence of distinct particles or morphologically defined material supports the hypothesis that the recruitment of the PNB material in DFC and GC occurs as large complexes.

Nucleolar Assembly

We found that fibrillarin concentrated in five NORs in telophase. We found that fibrillarin concentrated in five NORs in telophase. We predict that each HeLa-competent NOR associated with fibrillarin simultaneously in telophase. One of the six competent NORs is probably very weak, as has been shown for this HeLa cell line (Roussel et al., 1996), and cannot be detected by GFP. As G1 progressed, the time-lapse microscopy revealed both expansion of DFC and movement of the different NORs with respect to one another (Fig. 3 and Video 2). Concerning the formation of the GC, the Nop52-GFP signal was first associated with several NORs which then regrouped, resulting in the formation of a nucleolus (Fig. 9 and Video 7). The fusion of the GC was progressive and lasted several minutes even when the two NORs were in close contact. Redistribution of Nop52-GFP signals was visible after assembly into a single domain, reflecting the reorganization of the nucleolar components. This time-lapse microscopy study thus enabled us to illustrate for the first time in living cells that several NORs contribute to the formation of one nucleolus in human cells. Such NOR regroupment was not synchronous in the two daughter cells, indicating that this process may depend on the level of activity of these NORs. About 1 h later, after fusing, the nucleolus suddenly moved to a more central position in the nuclear volume, most probably due to reorganization of chromosome territories. Thus, the assembly of the nucleolus in HeLa cells, as summarized in Fig. 10, lasts 1.5 h from the beginning of anaphase and is associated with the interphase organization of the chromosome territories.

Discussion

How an Interphase Nucleus Forms in Living Cells

The contribution of the spatial organization of machineries to the regulation of nuclear activities is a fundamental concept (for reviews, see Lamond and Earnshaw, 1998; Lewis and Tollervey, 2000; Misteli, 2000) which is now being completed by studies in living cells (Sleeman and Lamond, 1999; Dundr et al., 2000; Eils et al., 2000; Gonzalez-

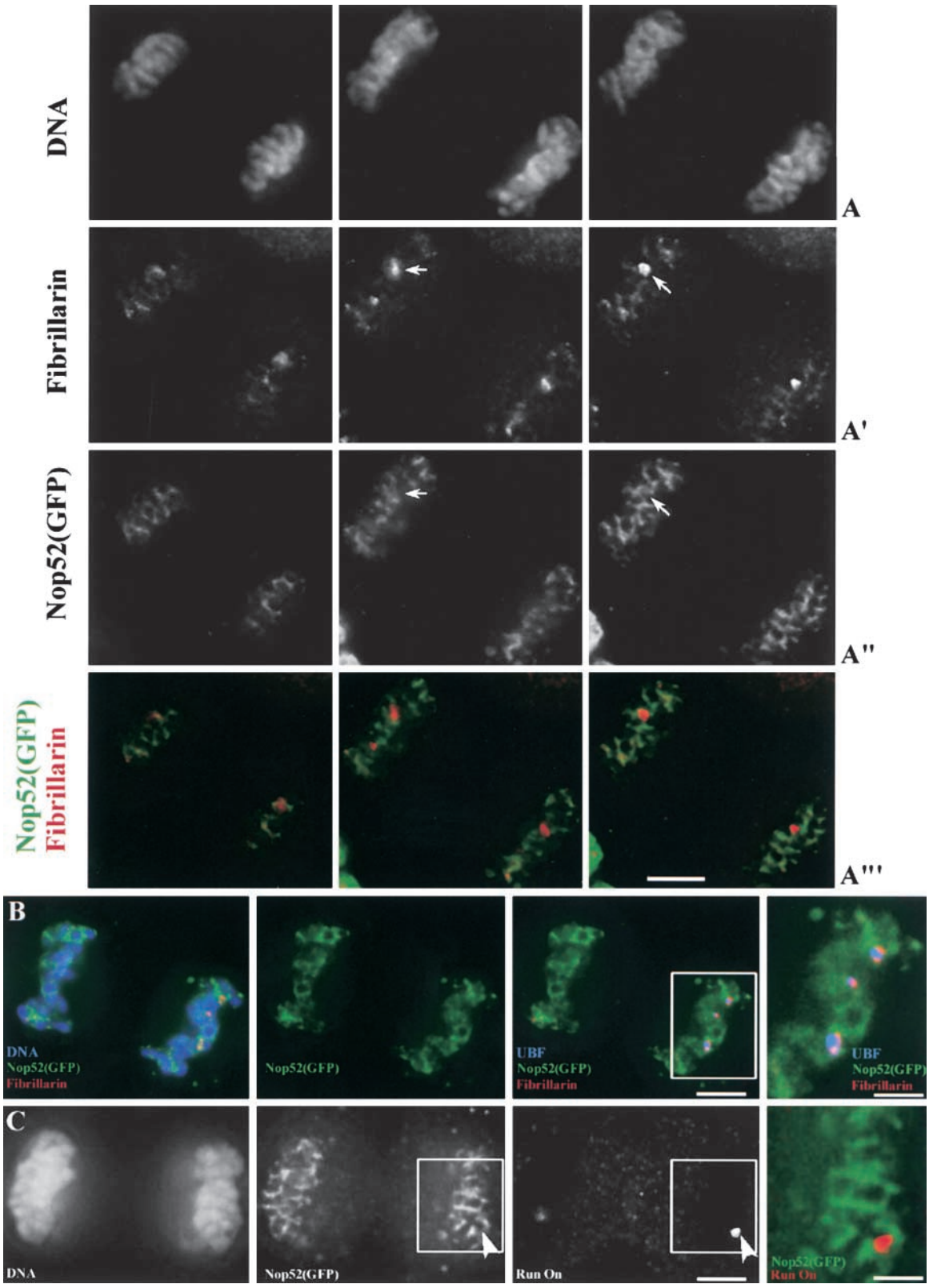

Figure 5. Relative distribution of Nop52 and fibrillarin in fixed cells in telophase. (A–A′′′) 55 focal planes of 0.2 μm of a fixed cell were recorded. Three focal planes are shown, the condensed chromatin is visualized (A) by DAPI, and fibrillarin is mostly accumulated in NORs (arrows) and to a lesser extent at the chromosome periphery (A′). However, Nop52-GFP remains underlining the chromosome periphery and accumulates in small foci that do not localize at NORs (A′′′); see merge (A′′′). See also Video 5. (B) Detection on a single optical section of UBF, fibrillarin, Nop52, and DNA. In merge, UBF colocalizes partially with fibrillarin at NORs whereas Nop52 is distributed at the chromosome periphery; see enlargement of the merge. (C) Detection by run on of RNA pol I transcription on a single optical section. RNA pol I transcription (arrowhead) is already active whereas Nop52 is still distributed at the periphery of condensed chromosomes; see enlargement of the signals visible in the square in the merged image. For 3-D cell reconstruction of panel A, see corresponding video. Bars, 10 μm and 5 μm in enlargements of B and C.

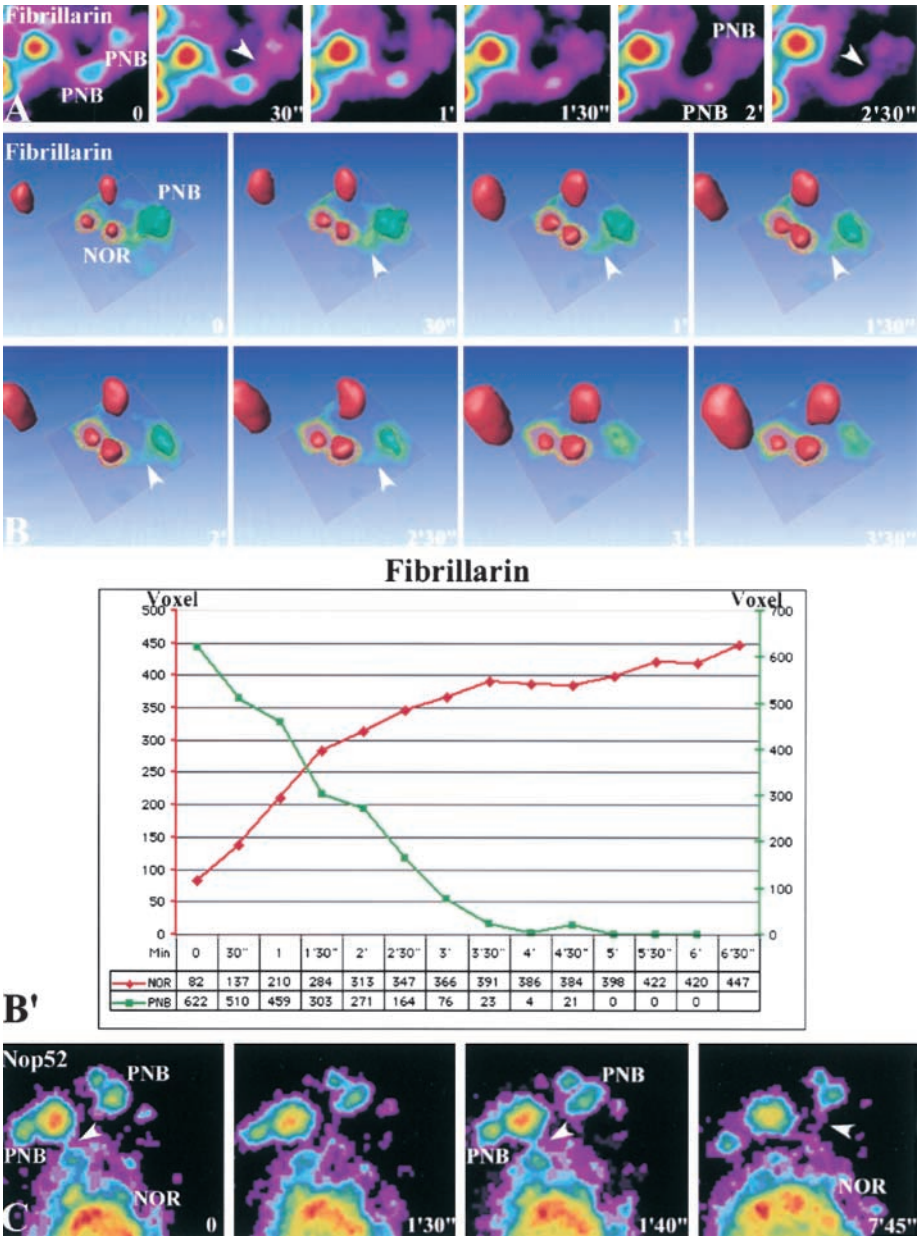

Figure 6. Protein delivery from PNBs to NORs/nucleoli and between PNBs. The delivery of material from PNBs to NORs is performed by flow (arrowheads); these flows do not last more than 2 min. This was observed for fibrillarin and Nop52 (A–C). (B) To better show the flow between PNB and NOR and quantify the volumes of these structures, we applied a surface rendering using Amira software (TGS). One of the two PNBs shown in panel A is selected and its interaction with the adjacent NOR was followed. The strong difference in intensity between PNB (displayed in green) and NOR (in red) constrained us to first isolate the PNB from the NOR and apply a different threshold adapted to the intensity of each structure. To show the material flow between PNB and NOR, we have also displayed in pseudocolor and isolines a plane in the stack containing this flow (B). See also Video 6. (B′) Volumes defined by the surfaces of the labeled NOR and PNB in B were measured in time and plotted in a graph that shows how the volume (in voxels) of the NOR increases whereas that of the PNB decreases. See corresponding video for dynamic visualization. For Nop52 (C), flows are also observed, connecting the PNBs with the nucleolus. Finally, the signal decreases in the emptying PNB and increases in the NOR (A–C); compare fibrillarin at times 0 and 2 min, and Nop52 at times 1′40″ and 7′45″.

Melendi et al., 2000; Phair and Misteli, 2000; Platani et al., 2000). Consequently, one of the remaining challenges is to understand how nuclear domains are formed in living cells. Redistribution of nuclear machineries at the time of nuclear reassembly has so far mainly been documented in fixed cells, making it impossible to determine the precise timing of nuclear domain formation, as well as to describe the events that trigger nuclear body formation. In fact, such temporal and spatial investigations depend on the ability to integrate signals within the total cell volume because the mitosis/interphase transition is characterized by important variations in cell shape. In this investigation, benefiting from the new possibilities offered by fast 4-D imaging, we provide information on the behavior of two proteins (fibrillarin and Nop52) representative of two functional domains of the nucleolus (DFC and GC) at the exit of mitosis. The advantage of the fast 4-D imaging technology is to permit the analysis of the formation and movement of large complexes during cell cycle progression, and consequently is appropriate to follow recruitment in space and time of nuclear machineries in living cells.

In living cells, the perichromosomal compartment follows the rapid migration of chromosomes to the poles. Contrary to yeast, the nucleolus does not persist during mitosis in higher eucaryotes, but the perichromosomal compartment containing a large number of nucleolar proteins might play this role. Interestingly, the two nucleolar proteins studied here belong to the DFC and the GC, respectively, and are representative of these nucleolar domains which are also the sites of sequestration of a cell cycle regulator, CdK14, in yeast (Granot and Snyder, 1991; Straight et al., 1999). It might well be possible that this continuous layer, strongly linked with condensed chromatin, could play an analogous role as a specific cell compartment sequestering regulatory cell cycle proteins normally

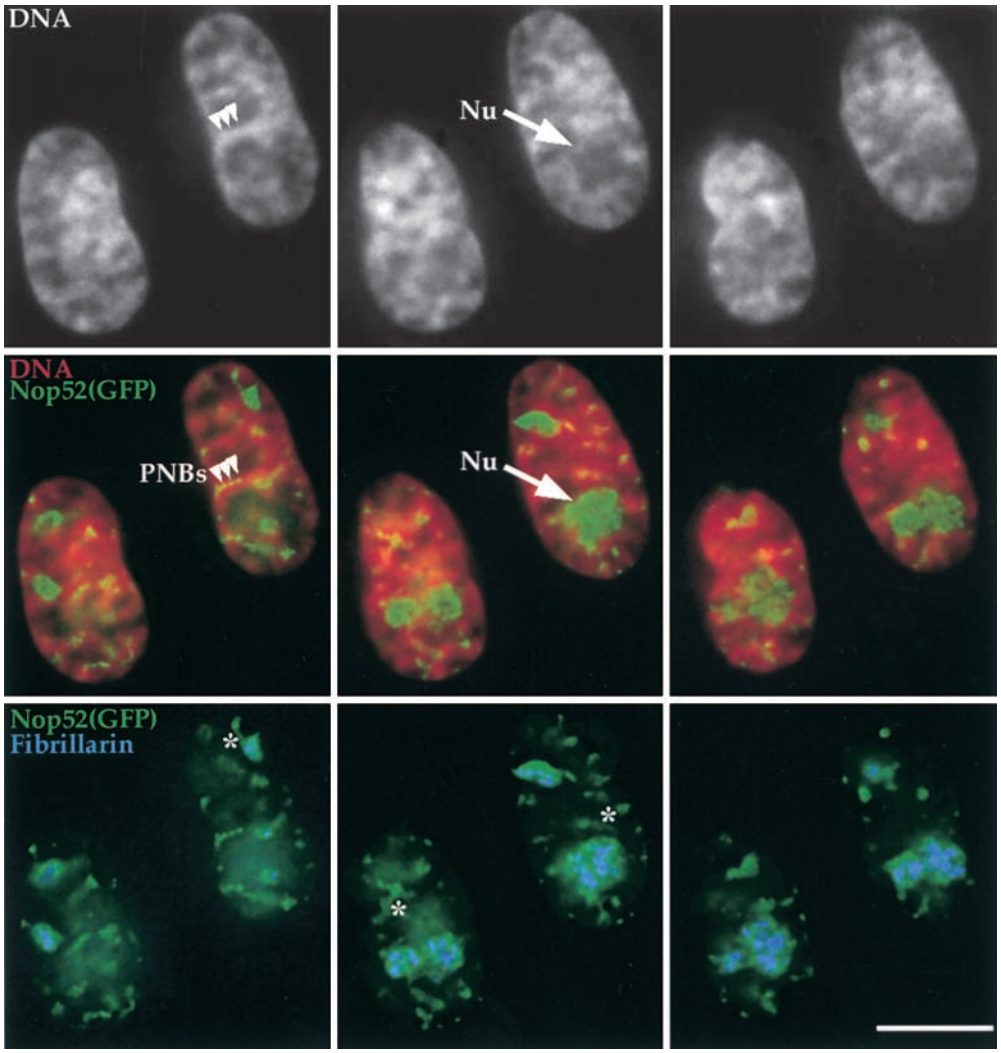

Figure 7. Distribution of Nop52 in fixed cells compared with DNA condensation and fibrillarin in G1 cells. Three different planes are shown. G1 cells still show some chromosome condensation as observed by DNA specific coloration. A merge of the DNA (red) and Nop52 (green) shows that Nop52 localizes in the nucleolus and in PNBs aligning on partially condensed chromatin (arrowheads); protein bridges are observed between PNBs and nucleoli (*). Fibrillarin (blue) exclusively accumulates in the nucleolus colocalizing only partially with Nop52. Nucleoli (Nu) localize in areas of faint DNA staining. Bar, 10 μm.

associated with the nucleolus during mitosis in yeast (Visitin and Amon, 2000).

The progression of nucleolar proteins towards the poles reflects their link with the chromosome periphery. This indicates that decrease of CdK1 activity at the onset of anaphase (Clute and Pines, 1999) has no effect on the linkage of nucleolar proteins at the chromosome periphery during the 4 min of migration. In telophase, decreasing of CdK1 activity (Sirri et al., 2000) overcomes the mitotic repression of RNA pol I transcription (Roussel et al., 1996; Fomproix et al., 1998; Dousset et al., 2000). It is precisely at that time that fibrillarin detaches from the chromosome surface to concentrate in PNBs and NORs. PNB-containing Nop52 appeared only 12 min after the onset of anaphase, almost exclusively at the chromosome surface and without detectable recruitment in NORs. Thus, it appears that Nop52 anchoring at the chromosome surface is regulated differently with regard to fibrillarin. Moreover, the delay of its recruitment in PNBs indicates the existence of other regulatory pathways in addition to the CdK1 pathway.

PNBs

PNBs are distinct nuclear structures scattered throughout the nucleus in early G1 (Stevens, 1965). They correspond to preassembled nucleolar RNP complexes involved in processing steps of rRNAs (Ochs et al., 1985; Benavente et al., 1987; Jiménez-Garcia et al., 1994; Dundr et al., 1997; Mukharyamova et al., 1999; Savino et al., 1999; Dundr et al., 2000; Verheggen et al., 2000). The prevailing model is that PNBs move to sites of active pre-rRNA transcription after mitosis, i.e., at transcribing NORs (Benavente et al., 1987; Benavente, 1991; Jiménez-Garcia et al., 1994).

However, the mobility of the PNBs was recently questioned and it was proposed that they are in a continuous state of flux because, in experiments using fluorescence recovery after photobleaching (FRAP), fibrillarin-GFP diffuses from PNBs and rapidly reassociates with them (Dundr et al., 2000). In this work, by 4-D imaging we investigated cells from metaphase to G1 to determine in liv-

Figure 8. Structure of PNBs and modifications at the proximity of the nucleolus. Two early G1 Nop52-GFP HeLa cells are seen in phase contrast (A). Bar, 8 μm. The lefthand daughter cell is observed by fluorescence microscopy (A′): Nop52-GFP accumulates in the newly formed nucleolus and in seven PNBs, five of which are indicated by arrowheads. Bar, 2 μm. (A″) In an ultrathin section showing the same focus level as A′, the positions of the nucleolus and of the same five PNBs (arrowheads) are eas-

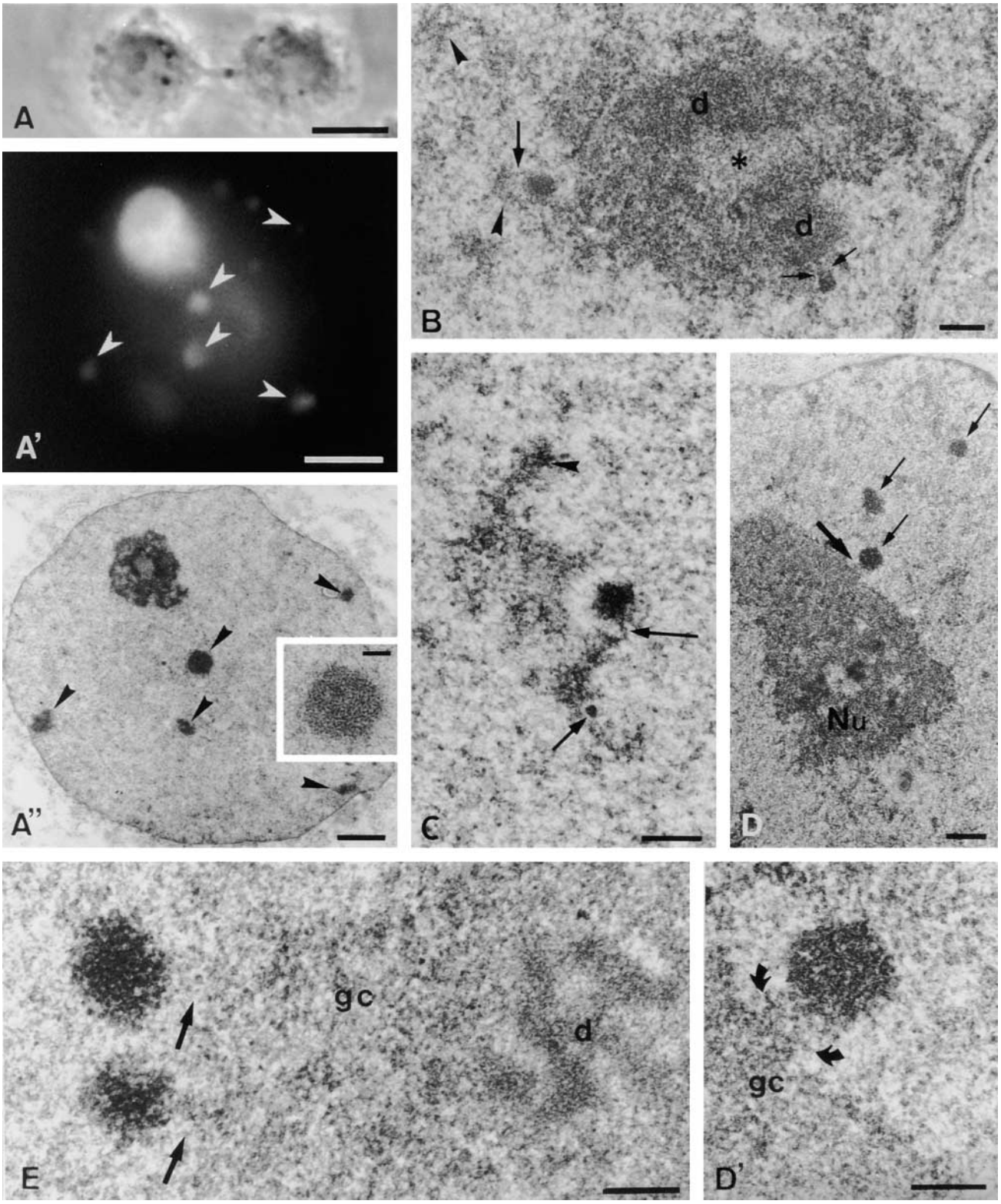

ily identified. Bar, 1 μm. Inset: detail of the central PNB with a fibrillogranular structure. Bar, 0.2 μm. (B–E) Electron micrographs of HeLa cell nuclei. (B) Late telophase. The chromatin (arrowheads) is decondensing and two PNBs are seen in the vicinity of the reforming nucleolus. The larger PNB is linked (arrow) to the condensed chromatin, and the connection between the smaller PNB and the DFC (d) is seen between the two arrows; fibrillar center (asterisk). Bar, 0.2 μm. (C) Early G1. A PNB appears linked to the condensed chromatin (arrowhead) via thin fibrils (long arrow); perichromatin granule (short arrow). Bar, 0.2 μm. (D) Early G1. Three PNBs are seen (thin arrows), one of them attached (thick arrow) to the nucleolus (Nu). Bar, 0.5 μm. (D′) Detail of the contact PNB-nucleolus, observed in D; note the granular material (between arrows) forming the link between the PNB and the GC (gc). Bar, 0.2 μm. (E) G1 phase. Two PNBs are associated with a nucleolus completely reformed. GC (gc); DFC (d). Material in the link (arrows), appears more diffuse than in D′. The top PNB is mainly composed of granules. Bar, 0.2 μm.

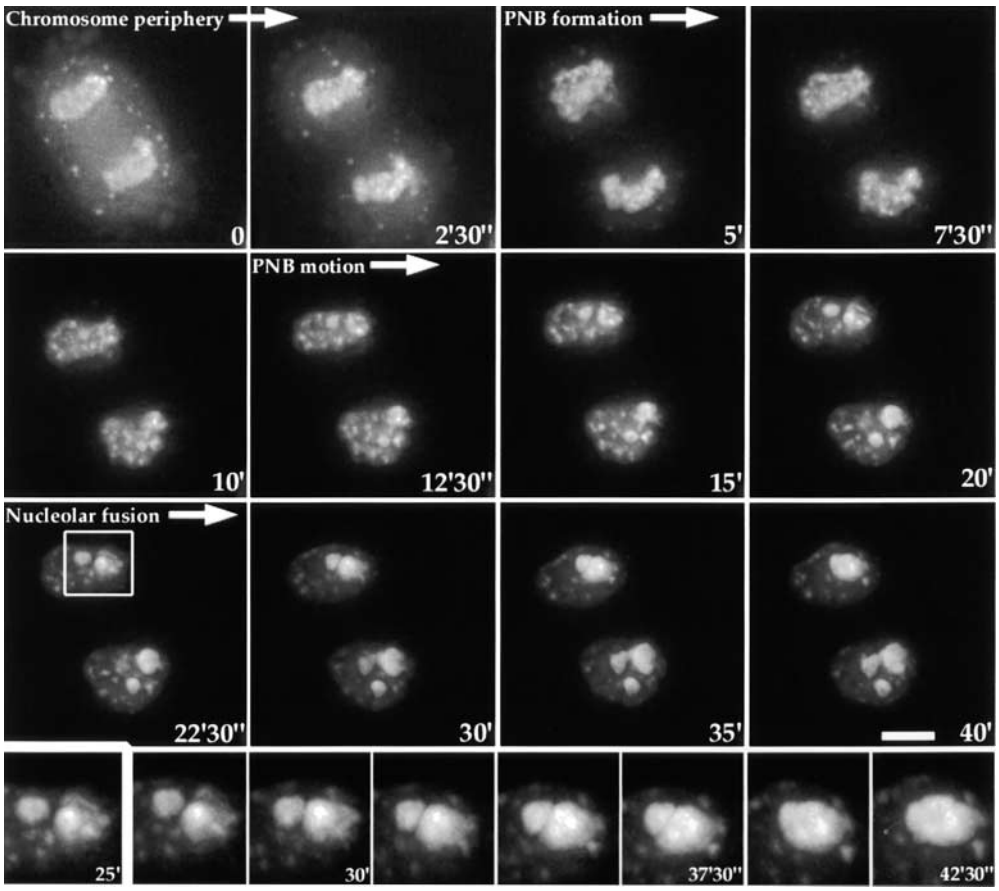

Figure 9. From telophase to an interphasic nucleolus. Time lapse sequence, with a 2.5-min frequency, shows the dynamics of Nop52 from the periphery of the chromosome, to PNB formation, and assembly in NORs followed by fusion of nucleoli. A detail of this fusion is also shown (inset). Bar, 10 μm. See also video 7 for 3-D nucleolar reconstruction and fusion of nucleoli in G1 phase.

ing cells how nuclear bodies such as PNBs are formed and recruited to specific genes at the beginning of interphase. Advantage was also taken of stable transfected cell lines for which evidence is provided that nucleolar formation occurs as in control cells, and this enabled us to analyze protein dynamics during the transition mitosis/interphase.

Fibrillarin and other nucleolar proteins are believed to be constantly diffusing into the nucleus (Dundr et al., 2000;

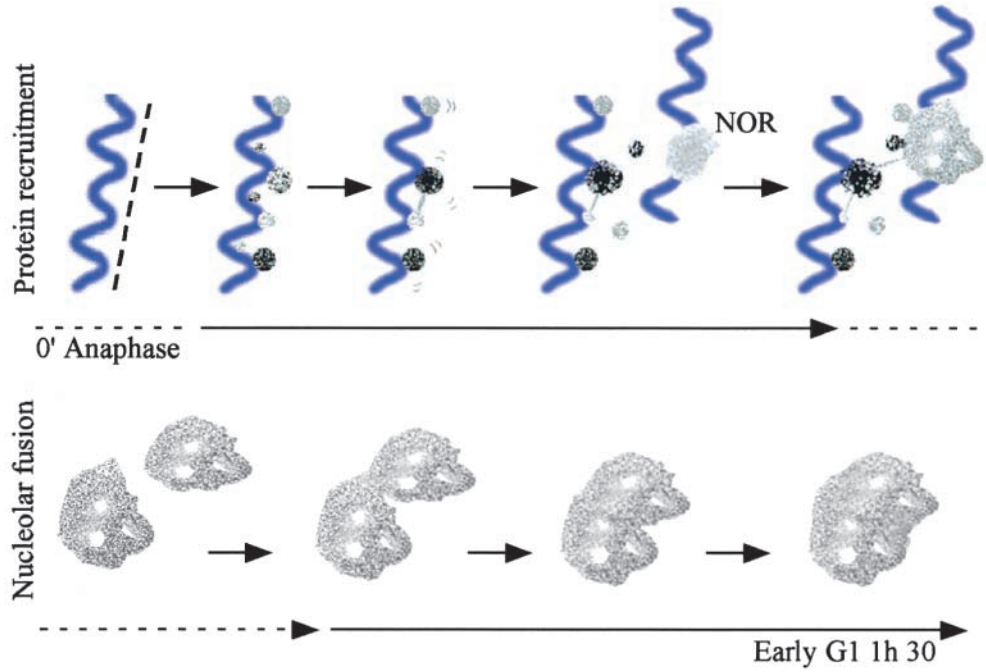

Figure 10. Schematic reconstruction of the nucleolus. Proteins at the periphery of chromosomes (dashed line) assemble in PNBs attached to condensed chromatin (blue), and movements on the spot of these PNBs are observed (videos from Figs. 2–4 and 9). Different types of PNBs coexist in the nucleoplasm (gray or black). As the chromatin decondenses (not represented), some PNBs come into contact with newly forming nucleoli (NOR) and deliver their protein content; feeding from one PNB to another also exists. Several nucleoli are formed at this time and can fuse to one another. A certain lapse of time is required until the nucleolar components reorganize after the fusion (see Fig. 9 for how this distribution evolves in time for Nop52, a GC protein).

Phair and Misteli, 2000), yet associate first in PNBs before being directed to and retained in the nucleolus. Our time-lapse microscopy analysis reveals increasing accumulation of fibrillarin simultaneously in short-lived PNBs (mean life time: 15 min) and in NORs, and accumulation of Nop52 in long-lived PNBs (mean life time: 80 min) and later in NORs. A reasonable explanation could be that the retention of these nucleolar proteins at these sites is due to molecular interactions. We propose that pre-rRNAs can play such a role because some are known to pass through mitosis in association with nonribosomal proteins and are localized at the chromosome periphery and in PNBs (Dundr and Olson, 1998; Pinol-Roma, 1999; Dousset et al., 2000; Dundr et al., 2000). Moreover, it has been reported that the physical association of these proteins in large complexes is largely mediated by rRNA (Pinol-Roma, 1999).

Interestingly, it was found that the decrease of CdK1 activity in telophase (Clute and Pines, 1999) activates RNA pol I transcription and also induces the degradation of mitotic pre-rRNAs (Sirri et al., 2000). Differential instability of these mitotic pre-rRNAs could explain the progressive dissociation of distinct PNBs. For example, the persistence of the PNB-containing Nop52 could be related to the maintenance of partially cleaved pre-rRNAs. Nop52 is known to be involved in ITS2 processing and could remain associated with the ITS2 sequence during mitosis. This hypothesis is supported by the fact that pre-rRNAs as well as rRNA processing intermediates were found associated with immunopurified complexes from mitotic cells (Pinol-Roma, 1999). This scenario has the advantage of explaining both transient retention of fibrillarin and Nop52 in PNB-containing pre-rRNA, and more stable residence in transcribing NORs containing more permanent pre-rRNA. Moreover, we recently found a link between the presence of pre-rRNAs and the regroupment of PNBs around the NORs (Verheggen et al., 1998; 2000). Furthermore, in early G1 actinomycin D–treated cells, protein recruitment occurs at NORs as well as in PNBs but these PNBs are larger than in transcribing cells (Zatsepina et al., 1997; Dousset et al., 2000). Moreover, these large PNBs appeared immobile by time-lapse microscopy (our unpublished observation). Thus, under RNA pol I inhibition, the dynamics of recruitment into the nucleolus are reduced; this is best explained by the absence of accumulation of proteins in nucleoli and consequently accumulation and retention in PNBs. The hypothesis of PNB formation around preexisting mitotic pre-rRNAs remains to be proven. However, this could explain the temporal order of nucleolar delivery of the processing machinery driven by pre-rRNA stability.

Reaching Ribosomal Genes and the Nucleolus

Contrary to the established dogma, the absence of directional PNB movement could not explain the progressive concentration of nucleolar proteins into the nucleolus. It was recently reported that PNBs exhibited very little movement and disappeared (Dundr et al., 2000). As observed here by 4-D imaging, we confirm the observation that PNBs do not move in the nuclear volume and demonstrate that their disappearance is not the consequence of their relocation out of the focal plan. The detailed analysis of events happening at neighboring PNBs suggests an alternative explanation consisting of a dynamic delivery from one PNB into another neighboring PNB and from PNBs into the nucleolus via connections of unknown nature. The dynamics of assembly and disassembly of PNBs and the predominant accumulation of proteins in the more stable NORs could control this directional nuclear traffic. It is known from photobleaching recovery assays that there is permanent nuclear diffusion of proteins, even those resident in the nucleolus such as fibrillarin (Dundr et al., 2000; Phair and Misteli, 2000).

In this study we demonstrate that there is in addition a directional delivery between PNBs, as well as between PNBs and the nucleolus. This link between PNB-containing nucleolin-GFP and nucleoli was also observed in CMT3 cells (Dundr et al., 2000) and therefore could not be a characteristic of HeLa cells. The electron microscopy observations showed organized structures forming bridges, in favor of the transmission of large complexes. We can only speculate on the molecules responsible for the formation of the bridges and their directionality. Simple diffusion can explain part of the nuclear traffic of nucleolar proteins (Dundr et al., 2000; Phair and Misteli, 2000), but an ordered pathway may also be considered to explain the recruitment of nuclear machineries at the exit of mitosis.

The PNBs display variable ultrastructures, reflecting different concentrations and associations of their components especially in the form of granules comparing early and late PNBs (Verheggen et al., 2000, and this study). Our findings support the hypothesis that PNBs could be assembly platforms for different nucleolar RNP complexes rather than mobile carriers involved in nucleolar delivery. Interestingly, the fact that we found stable connections between PNBs and condensed chromatin in interphase suggests that the PNBs which are assembled on the surface of chromosomes at the end of mitosis (this study) are located at the periphery of the chromosome territories at the beginning of interphase.

Forming a Nucleolus at the Beginning of Interphase

This in vivo investigation leads us to propose a new model (Fig. 10) in which the nuclear trafficking of PNBs is not responsible for delivery of nucleolar complexes into the nucleolus. Indeed, PNBs appear rather as sites of retention and assembly of different nucleolar RNP complexes. We hypothesize as already proposed (Dousset et al., 2000; Dundr et al., 2000) that differentially stable pre-rRNAs could be the molecules involved in the retention of nucleolar proteins in distinct PNBs as well as in the nucleolus.

In addition, we provide evidence for the first time that there is association of machineries and products stemming from different chromosome territories, i.e., different NOR-bearing chromosomes. The dynamics of nucleolar assembly is the following: initially five NORs recruit fibrillarin and DFCs expand progressively in early G1. Then GC complexes, reported by Nop52, associate with these five new nucleoli. The complete formation of the nucleoli is achieved when NORs move close together and integrate the GC in a single nucleolus. This sequence reveals the complexity of the phenomena involved in the 3-D organization of the interphase nucleus. They involve movement

of chromosome territories and demonstrate that products of different chromosome territories can associate in a common functional domain.

The authors are grateful to J.P. Aris for providing fibrillarin cDNA, S. Boeuf for help in cell culture, M.C. Gendron for cell sorting by FACS®, and M. Barre for photographic work. The authors wish to thank I. Sepulveda for his help in artwork. We thank A.-L. Haenni for critical reading of the manuscript.

This work was supported in part by the Centre National de la Recherche Scientifique and the Association pour la Recherche sur le Cancer (contract No. 9143 and No. 5304 to D. Hernandez-Verdun). T.M. Savino was a recipient of a Fellowship from Association pour la Recherche sur le Cancer.

Submitted: 14 August 2000
Revised: 2 April 2001
Accepted: 3 April 2001

References

Agard, D.A., Y. Hiraoka, P. Shaw, J.W. Sedat. 1989. Fluorescence microscopy in three dimensions. *Methods Cell Biol.* 30: 353–377.

Aris, J.P., and G. Blobel. 1991. cDNA cloning and sequencing of human fibrillarin, a conserved nucleolar protein recognized by autoimmune antisera. *Proc. Natl. Acad. Sci. USA*. 88:931–935.

Benavente, R. 1991. Postmitotic nuclear reorganization events analyzed in living cells. *Chromosoma*. 100:215–220.

Benavente, R., K.M. Rose, G. Reimer, B. Hügle-Dörr, and U. Scheer. 1987. Inhibition of nucleolar reformation after microinjection of antibodies to RNA polymerase I into mitotic cells. *J. Cell Biol.* 105:1483–1491.

Clute, P., and J. Pines. 1999. Temporal and spatial control of cyclin B1 destruction in metaphase. *Nat. Cell Biol.* 1:82–87.

Dousset, T., C. Wang, C. Verheggen, D. Chen, D. Hernandez-Verdun, and S. Huang. 2000. Initiation of nucleolar assembly is independent of RNA polymerase I transcription. *Mol. Biol. Cell*. 11:2705–2717.

Dundr, M., and M.O.J. Olson. 1998. Partially processed pre-rRNA is preserved in association with processing components in nucleolus derived foci during mitosis. *Mol. Biol. Cell*. 9:2407–2422.

Dundr, M., U.T. Meier, N. Lewis, D. Rekosh, M.-L. Hammarskjöld, and M.O.J. Olson. 1997. A class of nonribosomal nucleolar components is located in chromosome periphery and in nucleolus-derived foci during anaphase and telophase. *Chromosoma*. 105:407–417.

Dundr, M., T. Misteli, and M.O.J. Olson. 2000. The dynamics of postmitotic reassembly of the nucleolus. *J. Cell Biol.* 150:433–446.

Eils, R., D. Gerlich, W. Tvarusko, D.L. Spector, and T. Misteli. 2000. Quantitative imaging of pre-mRNA splicing factors in living cells. *Mol. Biol. Cell*. 11: 413–418.

Fomproix, N., and D. Hernandez-Verdun. 1999. Effects of anti-PM-Scl 100 (Rr6p exonuclease) antibodies on prenucleolar body dynamics at the end of mitosis. *Exp. Cell Res.* 251:452–464.

Fomproix, N., J. Gébrane-Younes, and D. Hernandez-Verdun. 1998. Effects of anti-fibrillarin antibodies on building of functional nucleoli at the end of mitosis. *J. Cell Sci.* 111:359–372.

Gébrane-Younès, J., N. Fomproix, and D. Hernandez-Verdun. 1997. When rDNA transcription is arrested during mitosis, UBF is still associated with non-condensed rDNA. *J. Cell Sci.* 110:2429–2440.

Gonzalez-Melendi, P., K. Boudonck, R. Abranches, B. Wells, L. Dolan, and P. Shaw. 2000. The nucleus: a highly organized but dynamic structure. *J. Microsc.* 198:199–207.

Granot, D., and M. Snyder. 1991. Segregation of the nucleolus during mitosis in budding and fission yeast. *Cell Motil. Cytoskelet.* 20:47–54.

Guarente, L. 1997. Link between aging and the nucleolus. *Genes Dev*. 11:2449–2455.

Hadjiolov, A.A. 1985. The nucleolus and ribosome biogenesis. Springer-Verlag, Wien/New York. 268 pp.

Isaac, C., Y. Yang, and T. Meier. 1998. Nopp140 functions as a molecular link between the nucleolus and the coiled bodies. *J. Cell Biol.* 142:319–329.

Jiménez-Garcia, L.F., M.L. Segura-Valdez, R.L. Ochs, L.I. Rothblum, R. Hannan, and D.L. Spector. 1994. Nucleologenesis U3 snRNA-containing prenucleolar bodies move to sites of active pre-rRNA transcription after mitosis. *Mol. Biol. Cell*. 5:955–966.

Jordan, P., M. Mannervik, L. Tora, and M. Carmofonseca. 1996. In vivo evidence that TATA-binding protein SL1 colocalizes with UBF and RNA polymerase i when rRNA synthesis is either active or inactive. *J. Cell Biol.* 133: 225–234.

Lamond, A.I., and W.C. Earnshaw. 1998. Structure and function in the nucleus. *Science*. 280:547–553.

Lewis, J.D., and D. Tollervey. 2000. Like attracts like: getting RNA processing together in the nucleus. *Science*. 288:1385–1389.

Matera, A.G. 1999. Nuclear bodies: multifaceted subdomains of the interchromatin space. *Trends Cell Biol.* 9:302–309.

Meinel, E.S. 1986. Origins of linear an non-linear recursive restoration algorithms. *J. Opt. Soc. Am*. 3:787–799.

Misteli, T. 2000. Cell biology of transcription and pre-mRNA splicing: nuclear architecture meets nuclear function. *J. Cell Sci.* 113:1841–1849.

Moore, G.P.M., and N.R. Ringertz. 1973. Localization of DNA-dependent RNA polymerase activities in fixed human fibroblasts by autoradiography. *Exp. Cell Res.* 76:223–228.

Mukharyamova, K.S., O.A. Doudnik, A.I. Speransky, and O.V. Zatsepina. 1999. Double immunolocalization of major nucleolar proteins, fibrillarin and B23, in dividing mammalian cultured cells. *Membr. Cell Biol.* 12:829–843.

Ochs, R.L., M.A. Lischwe, E. Shen, R.E. Caroll, and H. Busch. 1985. Nucleologenesis: composition and fate of prenucleolar bodies. *Chromosoma*. 92:330–336.

Olson, M.O.J., M. Dundr, and A. Szebeni. 2000. The nucleolus: an old factory with unexpected capabilities. *Trends Cell Biol.* 10:189–196.

Pederson, T. 1998. The plurifunctional nucleolus. *Nucleic Acids Res.* 26:3871–3876.

Phair, R.D., and T. Misteli. 2000. High mobility of proteins in the mammalian cell nucleus. *Nature*. 404:604–609.

Pinol-Roma, S. 1999. Association of nonribosomal nucleolar proteins in ribonucleoprotein complexes during interphase and mitosis. *Mol. Biol. Cell*. 10:77–90.

Platani, M., I. Golberg, J.R. Swedlow, and A.I. Lamond. 2000. In vivo analysis of Cajal body movement, separation, and joining in live human cells. *J. Cell Biol.* 151:1561–1574.

Politz, J.C., S. Yarovoi, S. Kilroy, K. Gowda, C. Zwieb, and T. Pederson. 2000. Signal recognition particle components in the nucleolus. *Proc. Natl. Acad. Sci. USA*. 97:55–60.

Reimer, G., K.M. Pollard, C.A. Penning, R.L. Ochs, M.A. Lischwe, H. Bush, and E.M. Tan. 1987. Monoclonal antibody from a (New Zealand black × New Zeeland White)F1 mouse and some human scleroderma sera target an Mr 34,000 nucleolar protein of the U3 RNP particle. *Arthritis Rheum.* 30: 793–800.

Richardson W.H. 1972. Bayesian-based iterative method of image restoration. *J. Opt. Soc. Am.* 62:55–59.

Roussel, P., C. André, L. Comai, and D. Hernandez-Verdun. 1996. The rDNA transcription machinery is assembled during mitosis in active NORs and absent in inactive NORs. *J. Cell Biol.* 133:235–246.

Roussel, P., C. André, C. Masson, G. Géraud, and D. Hernandez-Verdun. 1993. Localization of the RNA polymerase I transcription factor hUBF during the cell cycle. *J. Cell Sci.* 104:327–337.

Savino, T.M., R. Bastos, E. Jansen, and D. Hernandez-Verdun. 1999. The nucleolar antigen Nop 52, the human homologue of the yeast ribosomal RNA processing RRP1, is recruited at late stages of nucleologenesis. *J. Cell Sci.* 112:1889–1900.

Scheer, U., and R. Hock. 1999. Structure and function of the nucleolus. *Curr. Opin. Cell Biol*. 11:385–390.

Scheer, U., M. Thiry, and G. Goessens. 1993. Structure, function and assembly of the nucleolus. *Trends Cell Biol.* 3:236–241.

Shaw, P., and E. Jordan. 1995. The nucleolus. *Annu. Rev. Cell Dev. Biol.* 11:93–121.

Sirri, V., P. Roussel, and D. Hernandez-Verdun. 1999. The mitotically phosphorylated form of the transcription termination factor TTF-1 is associated with the repressed rDNA transcription machinery. *J. Cell Sci.* 112:3259–3268.

Sirri, V., P. Roussel, and D. Hernandez-Verdun. 2000. In vivo release of mitotic silencing of rDNA transcription does not give rise to pre-rRNA processing. *J. Cell Biol.* 148:259–270.

Sleeman, J.E., and A.I. Lamond. 1999. Newly assembled snRNPs associated with coiled bodies before speckles, suggesting a nuclear snRNP maturation pathway. *Curr. Biol.* 9:1065–1074.

Stevens, B. 1965. The fine structure of the nucleolus during mitosis in the grasshopper neuroblast cell. *J. Cell Biol.* 24:349–368.

Straight, A.F., W. Shou, G.J. Dowd, C.W. Turck, R.J. Deshaies, A.D. Johnson, and D. Moazed. 1999. Net1, a Sir2-associated nucleolar protein required for rDNA silencing and nucleolar integrity. *Cell*. 97:245–256.

Thiry, M., and G. Goessens. 1996. The nucleolus during the cell cycle. Springer-Verlag, Heidelberg, Germany. 146pp.

Verheggen, C., S. Le Panse, G. Almouzni, and D. Hernandez-Verdun. 1998. Presence of pre-rRNAs before activation of polymerase I transcription in the building process of nucleoli during early development of *Xenopus laevis*. *J. Cell Biol.* 142:1167–1180.

Verheggen, C., G. Almouzni, and D. Hernandez-Verdun. 2000. The ribosomal RNA processing machinery is recruited to the nucleolar domain before RNA polymerase I during *Xenopus laevis* development. *J. Cell Biol.* 149: 293–305.

Visitin, R., and A. Amon. 2000. The nucleolus: the magician's hat for cell cycle tricks. *Curr. Opin. Cell Biol.* 12:372–377.

Zatsepina, O.V., O.A. Dudnic, I.T. Todorov, M. Thiry, H. Spring, and M.F. Trendelenburg. 1997. Experimental induction of prenucleolar bodies (PNBs) in interphase cells: interphase PNBs show similar characteristics as those typically observed at telophase of mitosis in untreated cells. *Chromosoma*. 105:418–430.

Zolotukhin, A.S., and B.K. Felber. 1999. Nucleoporins Nup98 and Nup214 participate in nuclear export of human immunodeficiency virus type 1 Rev. *J. Virol.* 73:120–127.